High quality quasi-Bessel beam generated by round-tip axicon

Oto Brzobohatý, Tomáš Čižmár, and Pavel Zemánek[*]

Institute of Scientific Instruments of the ASCR, v.v.i.,
Academy of Sciences of the Czech Republic
Královopolská 147, 612 64 Brno, Czech Republic

[*] *Corresponding author: zemanek@isibrno.cz*

Abstract: We study theoretically and experimentally the spatial intensity distribution of the zero-order Bessel beam formed by the axicon which possess a rounded tip. Such a tip generates a refracted beam that interferes with the quasi-Bessel beam created behind the axicon. In turn an undesired intensity modulation occurs that significantly disturbs the unique properties of the quasi-Bessel beam - namely the constant shape of the lateral intensity distribution and the slow variation of the on-axis beam intensity along the beam propagation. We show how the spatial filtration of the beam in the Fourier plane improves this spatial beam distribution and removes the undesired modulation. We use an efficient numerical method based on Hankel transformations to simulate the propagation of the beam behind the axicon and filter. We experimentally measure the intensity distribution of the beam in many lateral planes and subsequently reconstruct the spatial intensity distribution of the beam. Computed and measured beam distributions are compared and the obtained agreement is very good.

OCIS codes: (070.0070) Fourier optics and signal processing; (070.6110) Spatial filtering; (140.3300) Laser beam shaping.

References and links

1. J. Durnin, J. J. Miceli, and J. Eberly, "Diffraction-free beams," Phys. Rev. Lett. **58**, 1499–1501 (1987).
2. G. Indebetouw, "Nondiffracting optical fields: some remarks in their analysis and synthesis," J. Opt. Soc. Am. A **6**, 150–152 (1989).
3. M. R. Lapointe, "Review of non-diffracting Bessel beam experiments," Opt. Laser Technol. **24**, 315–321 (1992).
4. D. McGloin and K. Dholakia, "Bessel beams: diffraction in a new light," Contemp. Phys. **46**, 15–28 (2005).
5. J. Durnin, "Exact solutions for nondiffracting beams. I. The scalar theory," J. Opt. Soc. Am. A **4**, 651–641 (1987).
6. G. Indebetouw, "Realization of general nondiffracting beams with computer-generated holograms," J. Opt. Soc. Am. A **6**, 1748–1754 (1989).
7. S. H. Tao, W. M. Lee, and X.-C. Yuan, "Dynamic optical manipulation with a higher-order fractional Bessel beam generated from a spatial light modulator," Opt. Lett. **28**, 1867–1869 (2003).
8. S. H. Tao, W. M. Lee, and X.-C. Yuan, "Comment on nondiffracting beams," Apl. Opt. **43**, 123–126 (2004).
9. J. H. McLeod, "The axicon: A new type of optical element," J. Opt. Soc. Am. **44**, 592–597 (1954).
10. A. G. Sedukhin, "Marginal phase correction of truncated Bessel beams," J. Opt. Soc. Am. A **17**, 1059–1066 (2000).
11. R. M. Herman and T. A. Wiggins, "Production and uses of diffractionless beams," J. Opt. Soc. Am. A **8**, 932–942 (1991).
12. J. Arlt and K. Dholakia, "Generation of high-order Bessel beams by use of an axicon," Opt. Commun. **177**, 297–301 (2000).
13. V. Jarutis, R. Paškauskas, and A. Stabinis, "Focusing of Laguerre-Gaussian beams by axicon," Opt. Commun. **184 1-4**, 105–112 (2000).

14. M. Lei and B. L. Yao, "Characteristics of beam profile of Gaussian beam passing through an axicon," Opt. Commun. **239**, 367–372 (2004).

15. Y. Zhang, L. Wang, and C. Zheng, "Vector propagation of radially polarized Gaussian beams diffracted by an axicon," J. Opt. Soc. Am. A **22**, 2542–2546 (2005).

16. T. Čižmár, V. Kollárová, Z. Bouchal, and P. Zemánek, "Sub-micron particle organization by self-imaging of non-diffracting beams," New. J. Phys. **8**, 43 (2006).

17. C. W. Zheng, Y. J. Zhang, and D. M. Zhao, "Calculation of the vectorial field distribution of an axicon illuminated by a linearly polarized Gaussian beam," Optik **117**, 118–122 (2006).

18. Y. Zhang, "Simple and rigorous analytical expression of the propagating field behind an axicon illuminated by an azimuthally polarized beam," Appl. Opt. **46**, 7252–7257 (2007).

19. Y. Zhang, "Analytical expression for the diffraction field of an axicon using the ray-tracing and interference method," Appl. Phys. B **90**, 93–96 (2008).

20. C. J. Zapata-Rodriguez and A. Sanchez-Losa, "Three-dimensional field distribution in the focal region of low-Fresnel-number axicons," J. Opt. Soc. Am. A **23**, 3016–3026 (2006).

21. J. P. Campbell and L. G. Dsehiazer, "Near fields of truncated-Gaussian apertures," J. Opt. Soc. Am. **59**, 1427–1429 (1969).

22. V. Nourrit, J.-L. de Bougrenet de la Tocnaye, and P. Chanclou, "Propagation and diffraction of truncated Gaussian beams," J. Opt. Soc. Am. A **18**, 546–556 (2001).

23. Z. Ding, H. Ren, Y. Zhao, J. S. Nelson, and Z. Chen, "High-resolution optical coherence tomography over a large depth range with an axicon lens," Opt. Lett. **27**(4), 243–245 (2002).

24. B. Depret, P. Verkerk, and D.Hennequin, "Characterization and modelling of the hollow beam produced by a real conical lens," Opt. Commun. **211**, 31–38 (2002).

25. A. E. Martirosyan, C. Altucci, C. de Lisio, A. Porzio, S. Solimeno, and V. Tosa, "Fringe pattern of the field diffracted by axicons," J. Opt. Soc. Am. A **21**, 770–776 (2004).

26. V. Garcés-Chávez, D. McGloin, H. Melville, W. Sibbett, and K. Dholakia, "Simultaneous micromanipulation in multiple planes using a self- reconstructing light beam," Nature **419**, 145–147 (2002).

27. V. Garcés-Chávez, D. Roskey, M. D. Summers, H. Melville, D. McGloin, E. M. Wright, and K. Dholakia, "Optical levitation in a Bessel light beam," Appl. Phys. Lett. **8**, 4001–4003 (2004).

28. T. Čižmár, V. Garcés-Chávez, K. Dholakia, and P. Zemánek, "Optical conveyor belt for delivery of submicron objects," Appl. Phys. Lett. **86**, 174,101:1–3 (2005).

29. B. P. S. Ahluwalia, X.-C. Yuan, S. H. Tao, J. Bu, H. Wang, X. Peng, and H. B. Niu, "Microfabricated-composite-hologram-enabled multiple channel longitudinal optical guiding of microparticles in nondiffracting core of a Bessel beam array," Appl. Phys. Lett. **87**, 084,104:1–3 (2005).

30. T. Čižmár, M. Šiler, and P. Zemánek, "An optical nanotrap array movable over a millimeter range," Appl. Phys. B **84**, 197–203 (2006).

31. P. Fischer, A. E. Carruthers, K. Volke-Sepulveda, E. M. Wright, C. Brown, W. Sibbett, and K. Dholakia, "Enhanced optical guiding of colloidal particles using a supercontinuum light source," Opt. Express **14**, 5793–5802 (2006).

32. J. Arlt, T. Hitomi, and K. Dholakia, "Atom guiding along Laguerre-Gaussian and Bessel light beams," Appl. Phys. B **71**, 549–556 (2000).

33. S. Schmid, G. Thalhammer, K. Winkler, F. Lang, and J. H. Denschlag, "Long distance transport of ultracold atoms using a 1D optical lattice," New J. Phys. **8**, 1–15 (2006).

34. K. Shinozaki, C. Q. Xu, H. Sasaki, and T. Kamijoh, "A comparison of optical second-harmonic generation efficiency using Bessel and Gaussian beams in bulk crystals," Opt. Commun. **133**, 300–304 (1997).

35. J. Arlt, K. Dholakia, L. Allen, and M. J. Padgett, "Efficiency of second-harmonic generation with Bessel beams," Phys. Rev. A **60**, 2438–2441 (1999).

36. J. Amako, D. Sawaki, and E. Fujii, "Microstructuring transparent materials by nondiffracting ultrashort pulse beams generated by diffractive optics," J. Opt. Soc. Am. B **20**, 2562–2568 (2003).

37. J. Ježek, T. Čižmár, V. Neděla, and P. Zemánek, "Formation of long and thin polymer fiber using nondiffracting beam," Opt. Express **14**, 8506–8515 (2006).

38. X. Tsampoula, V. Garcés-Chávez, M. Comrie, D. J. Stevenson, B. Agate, C. T. A. Brown, F. Gunn-Moore, and K. Dholakia, "Femtosecond cellular transfection using a nondiffracting light beam," Appl. Phys. Lett. **91**, 053,902:1–3 (2007).

39. T. Čižmár, "Optical traps generated by non-traditional beams," Ph.D. thesis, Masaryk University in Brno (2006). URL http://www.isibrno.cz/omitec/download.php?Cizmar_PhD_thesis.pdf.

40. J. W. Goodman, *Introduction to Fourier Optics* (McGraw-Hill, 1968).

41. V. Karásek, T. Čižmár, O. Brzobohatý, P. Zemánek, V. Garcés-Chávez, and K. Dholakia, "Long-range one-dimensional longitudinal optical binding," submitted to Phys. Rev. Lett .

1. Introduction

The ideal zeroth-order Bessel beam is a prominent example of so called "non-diffracting" beam [1]. Its lateral electric field distribution is described by the zeroth-order Bessel function of the first kind and this distribution is invariant along the beam propagation. Such idealized Bessel beams would be of infinite transverse extent and carry infinite amount of energy and, therefore, they cannot be generated experimentally. However, over a limited spatial range, an approximation to such idealized beam can be obtained. This is termed a "quasi-non-diffracting" beam or quasi-Bessel beam (QBB) [2–4]. Its transverse spatial extent is confined, the beam retains its transversal profile but the intensity varies over the axial range of the beam's propagation. Pioneering ways of QBB generation used a narrow circular slit illuminated with a collimated light. Since the slit was placed at the focal plane of a lens [1], the spherical waves propagating from the slit were transformed by the lens into collimated waves having the same axial component of their constituent wavevectors. The QBB may be considered as the result of the interference of such collimated waves. However, the efficiency of beam intensity transfer from the illuminating beam to the QBB was very low and, moreover, the amplitude of the generated QBB was modulated by the diffraction envelope of the slit [1,5]. Holograms can generate QBB with higher diffraction efficiency of $\sim 40.5\%$ [6–8] but the axial profile of the optical intensity is still diffraction modulated. An ideal conical lens (axicon) [9] provides a promising option for obtaining high-intensity QBB due to its high efficiency.

There are an increasing number of papers dealing with theoretical aspects of QBBs and attempts to tune their properties closer to those of an ideal non-diffracting beams (see for example Ref. [10] and references therein). Here we focus here only on axicon generated beams. More basic treatments of the axicon generated QBB ignore diffraction effects on the axicon edges, assume an ideally sharp axicon tip and – within the scalar description – deal with different spatial distributions of beams (i.e. Gaussian, Laguerre-Gaussian) incident on the axicon [11–14]. They show that the beam retains its lateral shape and size but its intensity varies smoothly along the propagation axis. Extensions to the vectorial descriptions for linearly, radially, or azimuthally polarized beams are known, too [15–19]. More complex models show that diffraction from the axicon edges causes noticeable modulation of the on-axis optical intensity along the beam propagation [4, 10, 20]. Fortunately this effect can be neglected if the waist of the Gaussian beam illuminating the axicon is less than half of the axicon radius [21, 22]. However the influence of imperfect tip of the axicon and its impact upon the generated QBB is rarely addressed in the literature [23–25] even though it also causes undesired axial modulation of the QBB. Numerous practical applications of the QBB are based on smooth lateral profile of optical intensity along the beam propagation, for example simultaneous micromanipulation or guiding of microparticles or atoms [16, 26–33], second harmonic generation [34, 35], optical coherence tomography over a large depth range [23], generation of waveguides [36, 37], and optoporation [38]. Therefore the suppression of the on-axis intensity oscillations and beam width variations is a crucial step to obtain the desired QBB properties and for more successful implementation of the beam.

2. Influence of the tip curvature on the quasi-Bessel beam axial intensity distribution

2.1. Quasi-Bessel beam

An ideal Bessel beam is formed when an axicon with a sharp tip (henceforth termed *perfect axicon*) and infinite extent is illuminated with a plane wave. Behind the axicon the wavevectors of refracted plane waves cover the surface of a cone with semi-apex angle α_0 (see Fig. 1) and the Bessel beam is a product of their interference. Consequently, the angular spectrum of such an ideal Bessel beam behind an ideal axicon with infinite aperture is described by a delta function

$\delta(\alpha - \alpha_0)$ where the α is the polar angle and α_0 is related to the axicon parameters as

$$\alpha_0 = \arcsin\left(\frac{n}{n_0}\cos\tau/2\right) + \frac{\tau - \pi}{2} \approx \frac{n - n_0}{n_0}\frac{\pi - \tau}{2}. \tag{1}$$

We denote n and n_0 as refractive index of the axicon and medium around the axicon, respectively, and τ as the apex angle of the axicon (see Fig. 1).

However if a perfect axicon is illuminated with a Gaussian beam, the plane wave spectrum behind the axicon is no longer a delta function and its extent increases with decreasing Gaussian beam waist w_0 [13, 39]. The result is that the "non-diffracting" beam behind the axicon does not have a uniform intensity distribution along its axis of propagation and exists only over a limited range $z_{max} = w_0 \cos\alpha_0/\sin\alpha_0$. Using the scalar description of the electric component of the beam one can obtain [39]

$$E(\rho, z) = E_0\sqrt{\frac{2\pi k z w_0 \sin\alpha_0}{z_{max}}}\exp\left(-\frac{z^2}{z_{max}^2} - \frac{\pi i}{4}\right)J_0(k\rho\sin\alpha_0)\exp(ikz\cos\alpha_0), \tag{2}$$

where k is angular wavenumber and ρ denotes radial distance from the optical axis z. The optical intensity distribution can be obtained using $I(\rho, z) = c\varepsilon_0|E(\rho, z)|^2/2$:

$$I(\rho, z) = \frac{4Pk\sin\alpha_0}{w_0}\frac{z}{z_{max}}J_0^2(k\rho\sin\alpha_0)\exp\left(-\frac{2z^2}{z_{max}^2}\right) \equiv I_0(z)J_0^2\left(2.4048\frac{\rho}{\rho_0}\right), \tag{3}$$

where P is the total power of the incident Gaussian beam and $\rho_0 = 2.4048/(k\sin\alpha_0)$ is the radius of the high intensity core of the QBB. An example of the axial and radial intensity profiles of such a QBB is shown in Fig. 1(A).

In the following discussion, we will neglect the diffraction from the axicon outer edges (which is justified for $w_0 < A/2$, where A is the axicon radius [21, 22]) and focus on the influence of the round tip of the axicon upon the final beam distribution. Let us assume that the shape of the axicon surface is a hyperboloid of revolution of two sheets (see inset in Fig. 1(B)). If we place the centre of coordinate system at the tip of the perfect axicon, the surface of hyperboloid of interest (for $z < 0$) is described by the following formula:

$$\frac{z^2}{a^2} - \frac{\rho^2}{b^2} = 1 \quad \text{giving} \quad z = -\sqrt{a^2 + \left(\frac{a\rho}{b}\right)^2}. \tag{4}$$

Since $b/a = \tan(\tau/2)$, where τ is the apex angle of the perfect axicon (angle between asymptotes of the hyperboloid), we can rewrite Eq. (4):

$$z = -\sqrt{a^2 + \frac{\rho^2}{\tan^2(\tau/2)}}. \tag{5}$$

The smaller the parameter a, the more closely the axicon approaches the ideal sharp shape of the "perfect axicon".

Intuitively one can expect that parts of the axicon that are placed radially far from the axis, contribute to QBB formed further from the tip. However the round tip will focus part of the incident Gaussian beam propagating closer to the optical axis and create a convergent (divergent) nearly-spherical wave behind the axicon. This wave interferes with the QBB behind the axicon which results not only in the significant modification of the field distribution near the axicon tip but also farther from the axicon. The axial component of the nearly-spherical wavevector is equal to k on the optical axis, whereas the axial component of the QBB is equal

to $k_z = k \cos \alpha_0$. Therefore, the two co-propagating waves with different wavevector lengths interfere on the optical axis and create a periodic modulation of the axial beam intensity with a period $\lambda / (1 - \cos \alpha_0)$. The depth of this modulation decreases at axial positions placed farther from the axicon because of the decreasing intensity of the diverging spherical wave (see Fig. 1(B)).
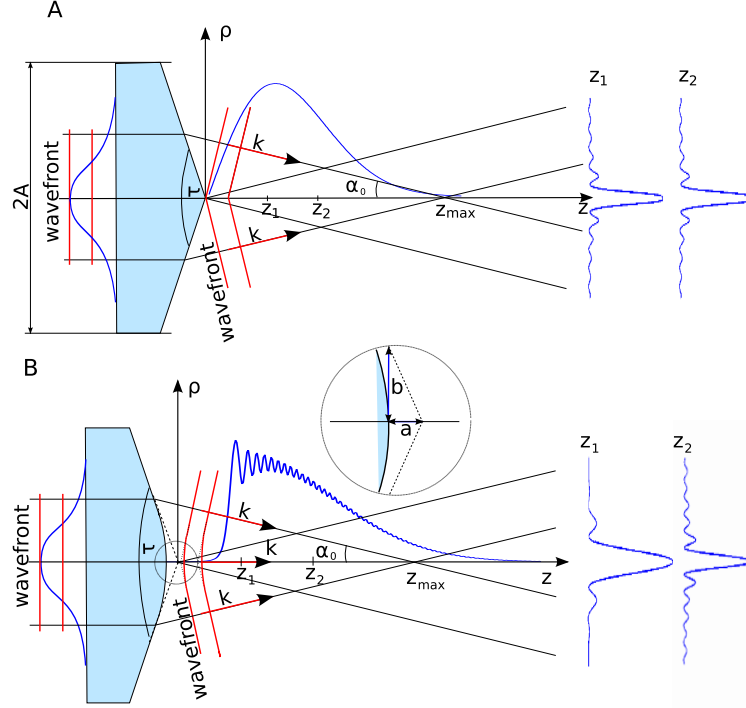

Fig. 1. A: Formation of a quasi-Bessel beam (QBB) by a perfect axicon illuminated by a Gaussian beam with a beam waist placed on the axicon front surface. The planar wavefronts of the Gaussian beam near the beam waist are denoted by straight red lines. Wavevectors **k** of the plane waves forming the QBB lie on the surface of a cone with semi-apex angle α_0. The intensity profile along the propagation axis is shown together with invariant shape of the radial profile at two axial positions z_1 and z_2. z_{max} is the maximum propagation distance where the QBB exists and τ is the apex angle of the axicon. B: Influence of the round axicon tip. New wave refracted by the round tip propagates behind the axicon and interferes with the QBB. This results in axial modulation of the optical intensity with a period $\lambda / (1 - \cos \alpha_0)$, where λ is the wave wavelength in the medium. Due to the interference the radial intensity distribution is no longer invariant (see examples at z_1 and z_2). Inset: Approximation of the round tip of the axicon by a hyperboloid of revolution of two sheets and the meaning of its parameters a and b.

2.2. Beam propagation behind a thin axicon

Let us assume that the axicon is illuminated with a Gaussian beam having its waist of width w_0 at the front axicon surface. Let us approximate the axicon as a thin lens and let us use the cylindrical system of coordinates (ρ, ϕ, z) having its origin at the tip of the perfect axicon with z axis following the beam propagation. Following [40] we obtain for the electric field just behind the axicon at z equal zero

$$E(\rho,0) = E_0 \exp\left(-\frac{\rho^2}{w_0^2}\right) \exp(\mathrm{i}kn\Delta_0) \exp\left[\mathrm{i}k(n_0-n)\sqrt{a^2+\frac{\rho^2}{\tan^2(\tau/2)}}\right], \qquad (6)$$

where Δ_0 is the maximum thickness of the axicon (on its axis) and k is the wavenumber.

Propagation of this field behind the axicon is obtained using the free-space propagation method based on decomposition of the field in plane $z = 0$ into a spectrum of plane waves (spatial-frequency spectrum obtained by the Fourier transform) [40]. In the case of a rotationally symmetrical field the two-dimensional Fourier transform reduces to the form of the zero order Hankel transform:

$$S(R,z) = S(R,0) \exp\left(\mathrm{i}kz\sqrt{1-R^2}\right), \qquad (7)$$

$$S(R,0) = k \int_0^\infty E(\rho,0)\rho J_0(kR\rho)\,\mathrm{d}\rho, \qquad (8)$$

where the coordinate R is the normalized wavevector projection onto the ρ coordinate ($R = k_\rho/k$).

For numerical treatment the integration in Eq. (8) of the field behind the axicon can be replaced by summation:

$$S_i^0 = k \sum_{j=1}^N E(\rho_j,0)\rho_j\Delta\rho_j J_0(kR_i\rho_j), \qquad (9)$$

where $\Delta\rho_j = \rho_{j+1} - \rho_j$ is the length of the j-th step in the radial direction and the superscript S^0 denotes the value of the z equal zero. The spatial-frequency spectrum of the propagating field at position z can be obtained from

$$S_i^z = S_i^0 \exp\left(\mathrm{i}kz\sqrt{1-R_i^2}\right). \qquad (10)$$

The resultant field is then obtained by the inverse Hankel transform of Eq. (10):

$$E_i^z = k \sum_{j=1}^N R_j\Delta R_j S_j^z J_0(kR_j\rho_i), \qquad (11)$$

where $\Delta R_j = R_{j+1} - R_j$.

Quantities ρ and R must be properly sampled especially in the vicinity of $\rho = 0$ and $R = 0$ and therefore parabolic sampling was chosen here:

$$N = k\rho_{\max}, \qquad (12)$$

$$\rho = \rho_{\max} \cdot \left[0,\ (1/N)^2,\ (2/N)^2,\ ...,1\right], \qquad (13)$$

$$R = \left[0,\ (1/N)^2,\ (2/N)^2,\ ...,1\right], \qquad (14)$$

where $\rho_{\max} \approx 2.5w_0$ is the boundary of the field in the direction perpendicular to the propagation direction.

In this numerical algorithm the Hankel transform is performed by the multiplication of $N \times N$ matrix $kJ_0(kR_i\rho_j)$ and a $1 \times N$ vector $E_j\rho_j\Delta\rho_j$ (see the source code of Section 2.4 in [39]). Significant speed of computation using this algorithm is reached if the $N \times N$ matrix is evaluated at the beginning of the whole procedure and used whenever the Hankel transform is needed. However we note that the computer memory requirement increases with square of the size of the Gaussian beam waist w_0.
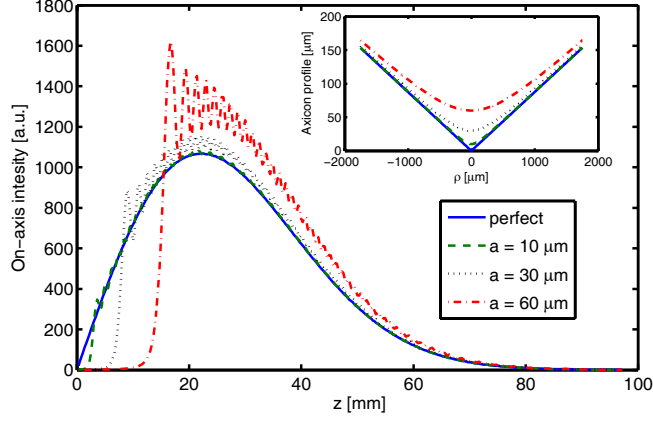
Fig. 2. Calculated axial optical intensity distribution behind the axicon with different values of axicon tip parameter a illustrated in the inset. The intensity distribution for the perfect axicon ($a = 0$ μm) is plotted as a full line. With increasing a the spatial distribution of the optical intensity is significantly disturbed. The presented results were calculated for the Gaussian beam waist $w_0 = 2140$ μm, wavelength $\lambda_{\mathrm{vac}} = 1064$ nm, apex angle of the axicon $\tau = 170°$, and axicon refractive index $n = 1.50669$.

Application of this algorithm to the beam propagation behind the round tip of the axicon is shown in Fig. 2. The intensity maximum is clearly shifted further from the axicon due to the partial focusing of the wave by the axicon tip. The periodic modulation of the axial intensity distribution is clearly visible and it significantly disturbs the QBB distribution over approximately the first half of the range of its existence behind the axicon.

The influence of the axicon tip parameter a on the axial optical intensity is illustrated in Fig. 2. It can be seen that even relatively small value of $a = 60$ μm can create 50% deviation of the axial optical intensity from the expected ideal case. Moreover the slowly varying envelope is disturbed by oscillations with modulation depth reaching 25% of its maximal value.

2.3. QBB transformation by a telescope

The QBB obtained by an axicon usually has too large a central core diameter to be used for experiments at micro-level. Therefore a demagnifying telescope is often used (see Fig. 6).

The lenses forming the telescope were considered as phase masks and the field immediately behind the lens L_i was obtained from

$$E(\rho, z_{L_i}) = E_0(\rho, z_{L_i}) \exp\left(-i\frac{k}{2f_i}\rho^2\right), \tag{15}$$

where f_i was the focal length of the first ($i = 1$) and second ($i = 2$) lens in the telescope and z_{L_i} is its axial position. An example of such beam propagation behind the perfect axicon and through such a telescope is shown in Fig 3. The white curves show the numerically calculated axial intensity profiles.

2.4. Spatial filtration of disturbed QBB

The demagnifying telescope is mainly used for generation of narrow high intensity QBB. However the presence of such a telescope in the optical set-up generating QBB is highly advantageous for possible spatial filtration of the beam. The back focal plane of the first lens L_1
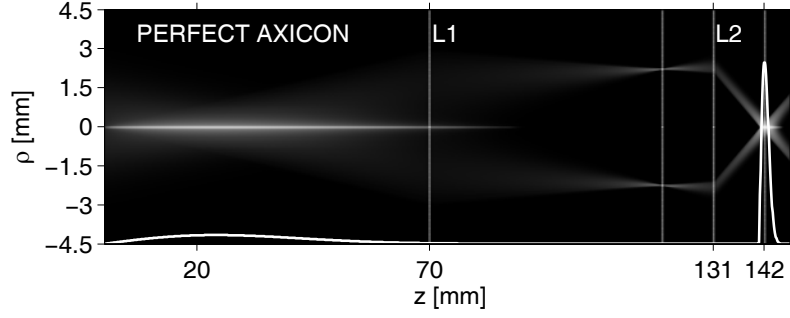
Fig. 3. A free-space propagation method was used to calculate the spatial optical intensity distribution of the field behind the perfect axicon illuminated by a Gaussian beam (beam waist $w_0 = 2140$ μm) at the wavelength $\lambda = 1064$ nm. The telescope is formed from lenses L_1 and L_2 of focal lengths $f_1 = 50$ mm and $f_2 = 11$ mm, respectively. The white curves show the numerically calculated axial intensity profiles.
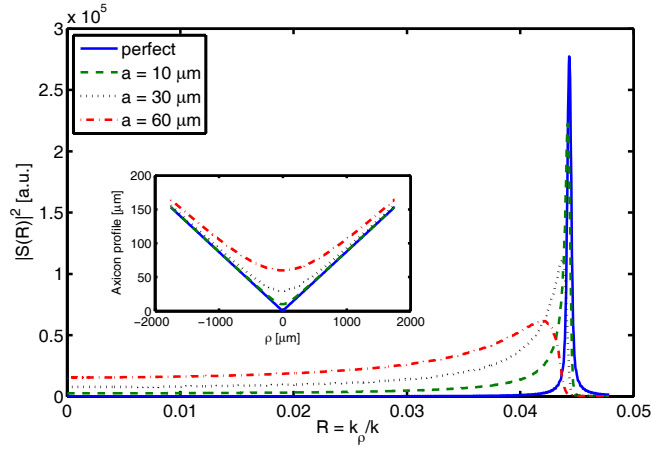

Fig. 4. The spatial-frequency spectrum $|S(R)|^2$ of the field behind the perfect axicon and axicon with round tip calculated for the Gaussian beam waist $w_0 = 2140$ μm, the wavelength $\lambda_{\text{vac}} = 1064$ nm and the apex angle of the axicon $\tau = 170°$, and axicon refractive index $n = 1.50669$. The hyperbolic shape of the axicon tip (see the inset) creates low frequency components in the spatial-frequency spectrum.

represents the Fourier plane where the spatial-frequency spectrum (SFS) of the QBB is formed. An example of such SFS is calculated in Fig. 4 for perfect axicon and round-tip axicon for three different a values. This figure clearly proves that the round-tip axicon creates low frequency components in SFS. An opaque circular obstacle (spatial filter) of proper radius placed into the back focal plane of the lens L_1 would block such unwanted low frequency components and therefore change the beam's spatial intensity distribution to resemble more closely that of a QBB produced by the perfect axicon. Radius of this spatial filter R_{f} can be predicted from Fig. 4 using $R_{\text{f}} = Rf_1$. As we demonstrate in Section 4 this simple modification suppresses the axial intensity oscillations and establishes the QBB propagating with unvarying width and slowly varying intensity envelope. Therefore the beam parameters are closer to the QBB generated by the perfect axicon.

3. Experimental arrangement

3.1. The axicon shape

We used axicon EKSPLA 130-0270 with apex angle $\tau = 170°$. The shape of its tip was measured by optical profilometer (MicroProf FRT, Fries Research & Technology GmbH) and it is shown in Fig. 5. We fitted the measured shape by a hyperboloid surface using Eq. (5) and we found $\tau = (169.81 \pm 0.01)°$ and $a_{\exp} = (33.7 \pm 0.1)\,\mu$m. Therefore τ coincides reasonably well with the value presented by the manufacturer.
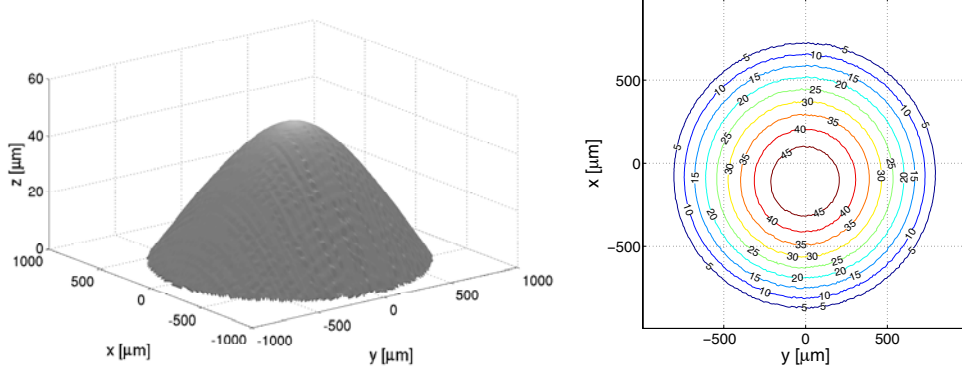
Fig. 5. Measured shape of the axicon and its contour plot.

3.2. Experimental set-up

Experimental setup for the QBB generation is depicted in Fig. 6. The incident Gaussian beam is transformed by an axicon. This beam is further demagnified by a telescope formed from lenses L_1 and L_2 to get a narrow QBB. This QBB is imaged on a CCD camera by an objective. The spatial filter (opaque circular obstacle placed in the back focal plane of L_1) was used to suppress the oscillations caused by the interference of the unwanted waves with the QBB. The filter was attached to a transparent window placed to the optical path and adjusted by XY micro-positioning stage.
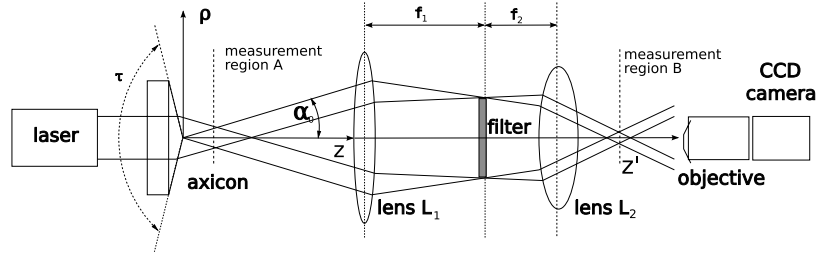

Fig. 6. Experimental set-up. Laser: IPG, YLM-10-1064-LP, wavelength 1064 nm, maximal power 10 W, beam-waist of incident Gaussian beam $w_0 = 2140\,\mu$m; axicon: EKSPLA 130-0270, apex angle $\tau = 170°$; lenses L_1, L_2: focal lengths $f_1 = 50$ mm and $f_2 = 11$ mm; objective: Mitutoyo M Plan Apo SL 80X; CCD camera: IDT X Stream VISION XS-3.

4. Comparison of theoretical and experimental results

4.1. Analysis of the original disturbed beam without filtering

In order to compare the theoretical predictions with the experimental beam distribution, we measured the lateral intensity distribution of the QBB behind the axicon and demagnified QBB behind the telescope. We imaged a number of lateral planes z_i (z_i') satisfying $z_{i+1} - z_i = 300\,\mu m$ behind the axicon ($z_{i+1}' - z_i' = 10\,\mu m$ behind the telescope) with a CCD camera. At each position z_i ten subsequent beam profiles were recorded and each of them was fitted by a formula based on Eq. (3):

$$I(\rho, z_i) = I_0(z_i) J_0^2 \left\{ 2.4048 \frac{\sqrt{[x - x_0(z_i)]^2 + [y - y_0(z_i)]^2}}{\rho_0(z_i)} \right\} + O(z_i), \qquad (16)$$

where $I_0(z_i)$, $x_0(z_i)$, $y_0(z_i)$, $\rho_0(z_i)$, and $O(z_i)$ are parameters of the fit at each z_i. The parameters $I_0(z_i)$ and $\rho_0(z_i)$ for all z_i give the axial dependencies of I_0 and ρ_0 of the QBB depicted in Figs. 7-8 as thin curves with plus marks (experiment). In order to compare this measurement with the theory presented in Section 2, we applied the parameters of the axicon we used (found in Section 3) in Eq. (6) and using Eqs. (9-11) we obtained the theoretical intensity distribution marked in Figs. 7-8 as full blue curves. Two experimental regions were studied: behind the axicon (measurement region A) and behind the demagnifying telescope (measurement region B). Intensity oscillations due to the round tip of the axicon are clearly visible in Fig. 7 in the high-intensity part of the beam for both measured and simulated data. The QBB core radii ρ_0 (see Eq. (16)) of the experimentally obtained and simulated QBBs are compared in Fig. 8. It is seen that the radius of the QBB core steeply decreases in the region of growing envelope of QBB intensity. Behind the intensity maximum the beam core radius of the measured beam varies in the range $9.54 \geq \rho_0 \geq 9.13\,\mu m$ and $2.50 \geq \rho_0 \geq 2.27\,\mu m$ for the measurement regions A and B, respectively. Figure 9 compares the measured and calculated 2D intensity distributions for the same parameters as in Fig. 7. The results prove that the chosen theoretical description of the problem is sufficient to obtain excellent coincidence with the measured results. Presented figures demonstrate serious variations of the beam generated behind round-tip axicon from the expected QBB distribution.
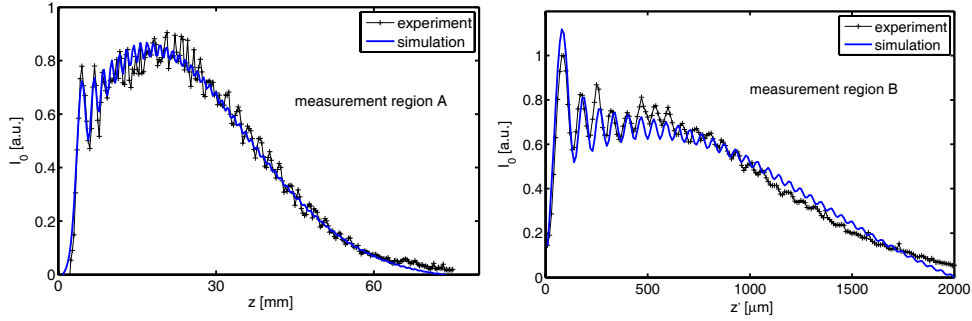

Fig. 7. Comparison of measured and calculated axial intensity profile I_0 of the QBB generated by the round-tip axicon measured directly behind the axicon (left - measurement region A in Fig. 6) and behind the demagnifying telescope (right - measurement region B).
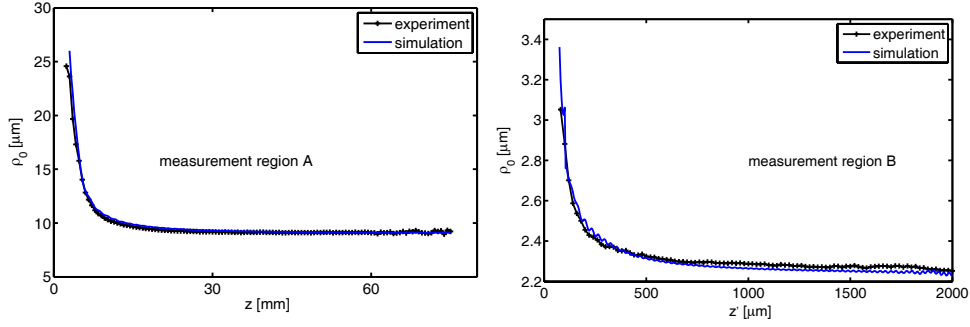
Fig. 8. Comparison of measured and calculated radius ρ_0 of the high intensity QBB core generated by the round-tip axicon measured directly behind the axicon (left) and behind the demagnifying telescope (right).
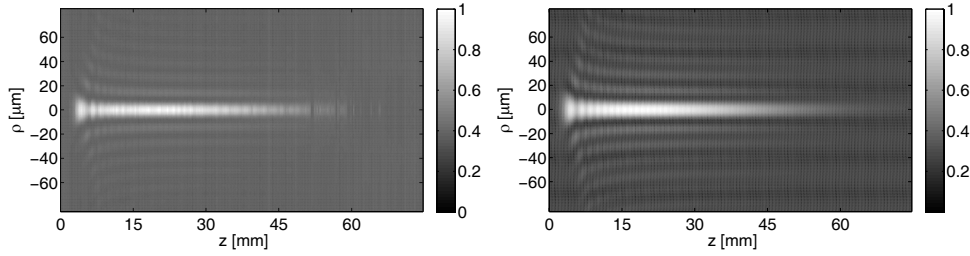

Fig. 9. The measured (left) and calculated (right) spatial intensity distribution of the QBB generated behind the round-tip axicon for the same parameters as in Fig. 7.

4.2. Analysis of the filtered beam

In order to optimize the size of the spatial filter we first simulated how the radius of the filter influences the final axial shape of the QBB generated by the round-tip axicon. We used the axicon parameters found in Section 3 $a = a_{exp} = 33.7\,\mu$m and put them into Eq. (6). Equations (9-11) gave the spatial intensity distribution with and without considered filters (see Fig. 10). It can be seen that the filtration does not give the same axial intensity profile as the ideal QBB and the total power in the beam decreases. However filters of radii larger than 2138 μm provide slowly varying axial intensity profiles without any oscillations over a distance of 2/3 z_{max}.

Figure 11 presents the measured axial intensity profile (I_0 in Eq. (16)) and radius of the QBB core (ρ_0 in Eq. (16)) if a filter of radius $R_{exp} = (1925 \pm 5)\,\mu$m was used (full curve). The full width at half maximum of this beam is still relatively high and is equal to 3/4 of the unfiltered beam. The overall intensity envelope is steeped but without sharp oscillations. The radii of the QBB core varies in the range $2.289 \leq \rho_0 \leq 2.245\,\mu$m all over the investigated axial region long 1.5 mm. This is $5\times$ less comparing to the beam radius variation without filter and considering only the axial region of the same length behind the intensity maximum mentioned above (see Fig. 7 and 8). Therefore the filtration improved lateral homogeneity of the beam, too. To compare this result with the theoretical simulations we again assumed $a = a_{exp} = 33.7\,\mu$m and searched for R_{fth} giving the best overlap with the measured axial intensity profile. The results are shown in Fig. 11 as a full blue curves. Even though we found $R_{fth} = (2115 \pm 5)\,\mu$m which is 10% larger than R_{exp}, we contend that the agreement is very good considering the sensitivity of the intensity distribution to the filter radius and the precision of its positioning between the lenses, each of relatively short focal length.
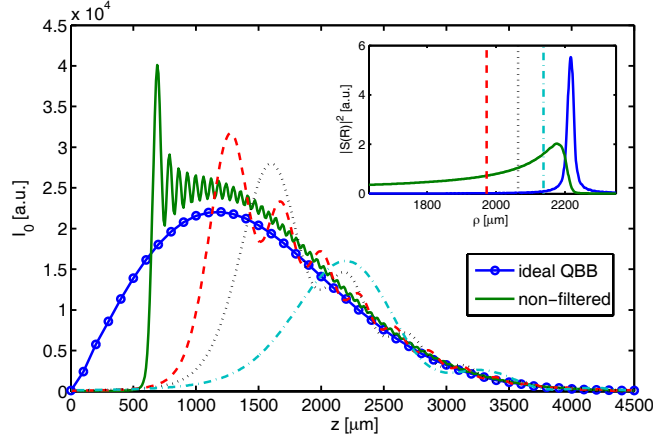
Fig. 10. Calculated axial intensity profile for perfect axicon (open circle with full line), and round-tip axicon with $a = 33.7$ μm. Different radii R_f of the spatial filter placed in the Fourier plane were considered: 0 μm (full), 1973 μm (dashed), 2064 μm (dotted), and 2138 μm (dot-dashed) (see the inset for corresponding spatial frequency spectrum cut-off).

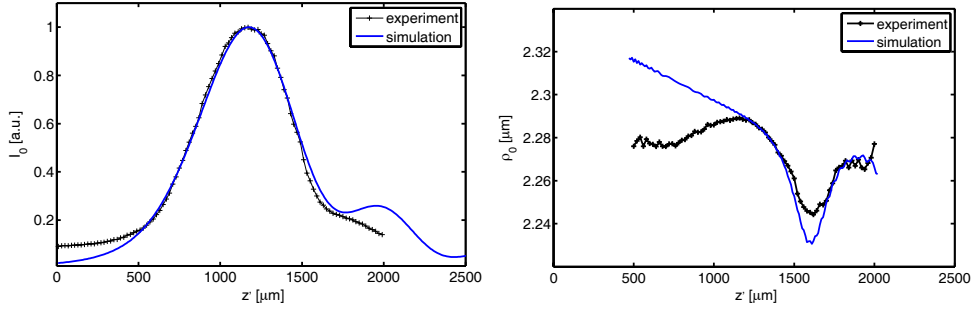Fig. 11. Comparison of measured (full with plus marks) and best fit calculated (full blue) axial intensity profiles I_0 (left) and beam core radii ρ_0 (right) for filtered QBB.

The measured and calculated 2D spatial intensity profiles of the filtered QBB generated behind the round-tip axicon are shown in Fig. 12. They clearly demonstrate that the spatial filtration method suppresses the unwanted oscillations and that the lateral shape of the beam does not vary along the beam propagation - similarly to the QBB generated by a perfect axicon.

5. Conclusions

We considered an imperfect axicon with round tip approximated by a hyperboloid of revolution of two sheets and we analyzed theoretically and experimentally the properties of the beam generated behind such an axicon. We demonstrated that if the axicon tip deviates in its apex from the ideal sharp tip in the range of tens of micrometers, the beam generated behind it does not possess the propagation invariant beam properties expected for quasi-Bessel beam. Severe axial oscillations of the optical intensity occur due to the interference between the quasi-Bessel beam, formed by off-axis part of the axicon, and the wave refracted by the round tip of the axicon. Such an intensity distribution can significantly influence experimental results expected for ideal quasi-Bessel beam and may cause artifacts for example in the measurement of weak
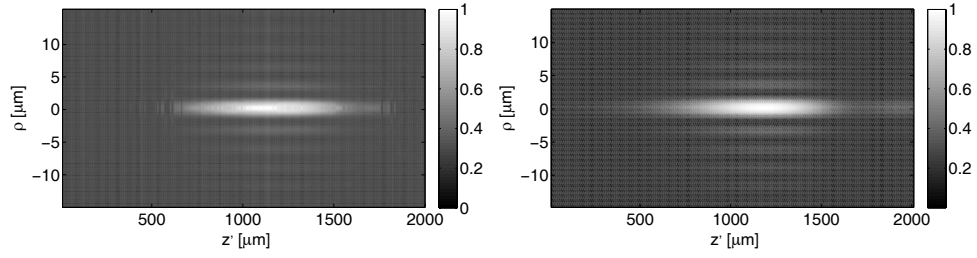
Fig. 12. The measured (left) and calculated (right) 2D spatial intensity profiles of filtered QBB generated behind the round-tip axicon. The parameters were the same as in Fig. 11.

inter-particle interactions in optical binding experiments [41]. We measured the real shape of the axicon, approximated the axicon tip by a hyperboloid, and found good coincidence between optical intensity distribution measured and theoretically simulated. We further demagnified the beam by a telescope and demonstrated how the spatial filtration of the beam in the telescope helps to remove the undesired modulation and establish the original invariant intensity beam distribution.

Acknowledgments